Power System Technology **Volume 46 · Number 4 · 2022**
ISSN: 1000-3673

Research on Vehicle-to-grid Process Based on System Dynamics

Cheng H., Shang Z., Guo Y., Kang C., Zeng W.
Department of Aerospace Engineering, University of Technology, Taiwan

ABSTRACT

Thermal radiation plays a key role in heat transfer between the flame and its surroundings. Measuring the radiation flux from the flame in the chamber is challenging due to the impact of the walls. Radiation emitted from the walls and the reflection of flame radiation from the walls interfere with the measurement of flame radiation. In this paper, various parameters that affect flame radiation are investigated. These studies are based on wall incident radiation and wall radiation heat flux. A theoretical method is proposed to calculate the flame radiation and compared it with the CFD simulation results to confirm its accuracy. The DO radiation model and a steady Flamelet combustion model with modified k-ε turbulence have been used to simulate the can-type combustion chamber. The CFD results were in good agreement with their theoretical ones, and the estimation of flame emission was accurately acceptable. It found out that in the entire temperature range of the wall temperature investigated in this type of combustion chamber, the radiation from the wall never deflects more than 10% of the flame radiation. Therefore, radiation heat transfer does not have a significant effect on the walls of the combustion chamber. Therefore, radiation heat transfer does not have a significant effect on the walls of the combustion chamber.

1. INTRODUCTION

Radiation heat transfer plays an essential role in heat transfer between the flame and its surroundings. Flame radiation caused by gas and particles is the dominant heat transfer mode in many combustion applications, such as industrial furnaces and coal-fired combustion boilers, and gas turbine combustors [1, 2].

While the measurement of flame radiation is simple in an open environment, it is challenging to do in a closed chamber because of the wall effect on flame radiation. The radiation emitted from the walls and radiation reflected from the walls by flame interrupts the measurement of the flame radiation[3]. One of the dominant complexities in calculating flame radiation is the configurations of radiation heat transfer like absorption coefficient, scattering coefficient of active optical gas components, and different combustion particles. [4-8].

The surface incident radiation received by the radiometer has three components on the inner surface of the combustion chamber:

1) Radiation emitted from the flame and combustion products (particles and optically active gases).
2) Radiation emitted from the walls.
3) Radiation reflected by the walls.

Besides, in all three mentioned cases, a part of receiving radiation is absorbed or scattered to the wall by gas or particle medium on its way.

Surface incident radiation, G_{total} , measured by radiometer can be defined as:

$$G_{\text{total}} = E_{\text{flame}} + G_{\text{wall}} \tag{1}$$

where in E_{flame} is flame radiation (direct radiation from the high temperature of combustion products that is partially absorbed or scattered by the medium), and G_{wall} is the contribution of wall emission and wall reflection.

To measure the flame radiation from incident radiation, some researchers detect it by measuring the difference in incident radiation with and without a flame (immediately after the flame is shut off) [9]. While in this approach, the influence of wall emission could be addressed, the effect of reflection from the wall is not predictable, which in some cases can affect the measurement of flame radiation.

In 2015, Kashir and co-workers modeled the swirled flame of SM1 for two turbulence models k-w-SST, and modified k-ε in different swirl numbers. After comparing the two models with experimental results in different temperatures and the mass fraction of fuel compartments like methane and carbon monoxide, they saw the results of the modified k-ε model closer to the experimental results [10].

In 2017, Fasihi and co-workers performed a study on radiation characteristics such as wall emissivity effect and gas scattering coefficient effect and study of wall effect on flame radiation for the Sydney burner. To minimize the wall effect on the flame radiation, they realized that the wall should be as well as possible at low temperatures and high emissivity. The results showed that when the difference between flame radiation and wall radiation is more than 25%, the wall emission rate is less than 0.8, and the wall temperature is more than 330K [11].

Table 1 summarizes previous studies that numerically examined radiation in a reactive combustion chamber. In many of these studies, the RANS model and the DO radiation model have been used.

Table 1: summery of numerical combustion chamber studies

No.	Author (Year)	Aim	Finding	Turbulence model	Radiation model	Ref.
1	Shakeel et al. (2017)	Reaction mechanisms and weighted sum of grey gas radiation models are examined to determine the most effective combination for numerical modeling of oxy-fuel combustion of methane in a gas turbine model combustor	The combinations of Jones-Lindstedt (5 equations) reaction mechanism and WSGGM model predicts the flame attachment to the fuel nozzle and gave the closest approximation to their experimentally observed combustor temperature profile.	Eddy Dissipation Concept (EDC)	WSGGM	[12]

No.	Author (Year)	Aim	Finding	Turbulence model	Radiation model	Ref.
2	Benini et al. (2009)	to evaluate the impact of increasing water and steam flows (ranging from 0% to 200% of the fuel mass flow) onto the emissions levels (NO and CO) of the engine.	thermal NO emissions decrease and, when steam is used, the appearance of a minimum in the amount of CO.	standard k-ε	p-1	[13]
3	Centeno et al. (2016)	A study of the effect of soot on the radiative heat transfer in a turbulent, nonpremixed methane–air flame inside a combustion chamber.	The radiation heat transfer was increased by 5.8% when radiation from soot was considered.	k-ε	DO	[14]
4	Datta et al. (1999)	Development of a numerical model of liquid fuel spray combustion in a gas turbine combustor to recognize the influence of inlet swirl number and combustion pressure on important combustion and emission characteristics	A relatively lower inlet pressure but a higher inlet swirl of incoming primary air will result in a better fuel economy, a more uniform exit temperature distribution along with a clean emission.	standard k-ε	WSGGM	[15]
5	Doner et al. (2013)	effect of non-grey gas analysis together with size parameter evaluated from actual particle size distribution of fly ash in the freeboard on incident radiative heat fluxes	Heat fluxes incident on the walls are significantly underpredicted in the absence of radiating particles in the medium. This finding indicates that the participating effect of the particles on the radiative heat fluxes is considerable.	-	DO	[16]

No.	Author (Year)	Aim	Finding	Turbulence model	Radiation model	Ref.
6	Krishna moorthy (2017)	The accuracies of the P_1 radiation model calculations were assessed by employing it in conjunction with a WSGGM an comparing its predictions against discrete ordinates (DO) model calculations in prototypical problems representative of modern combustion systems.	The optimized calculation times with the P_1 model were about 25–30% of the corresponding DO model solve times which were undertaken employing classical Gauss Seidel sweeps.	Large Eddy Simulations (LES)	P1	[17]
7	Rajpara et al. (2017)	proposes a reverse air flow arrangement for CAN type gas turbine combustor in order to minimize wall cooling requirements and NO_x emission level	The NO_x emission level is significantly low in proposed reverse air flow combustor compared to conventional combustor.	Large Eddy Simulations (LES)	DO	[18]
8	Sharma et al. (2004)	To improve the combustion process in order to achieve higher combustion efficiency, a desirable exit temperature and allowable liner wall temperature distribution and to reduce the combustion generated pollutants.	An increase in spray cone angle increases the bulk exit NO_x, though the increase is modest for higher volatile fuel. An increase in initial SMD increases the bulk exit NO_x for lower volatile fuels only.	standard k-ε	--	[19]
9	Yang et al. (2015)	To numerically investigate the effect of external surface emissivity on the flame-splitting limit of lean H_2/air mixtures in a micro cavity combustor.	The results show that the flame-splitting limit rises up with the decreasing of external surface emissivity. And it is revealed that the heat-loss ratio decreases as the surface emissivity is reduced, which gives rise to a more intense reaction in the cavity and a higher wall temperature level.	k-ε	DO	[20]

No.	Author (Year)	Aim	Finding	Turbulence model	Radiation model	Ref.
10	Zhi Yi et al. (2018)	The accuracy of no radiation, gray, gray-TRI and WSGG model is investigated based on the non-gray-TRI model (WSGG-TRI model)	When the radiation is neglected, the maximum temperature will rise by 130.7 K. On the contrary, when using the gray model, the maximum temperature will drop by 137.1 K, indicating that the gray model will exaggerate the impact of radiation.	standard k-ε	DO	[21]
11	Yilmaz et al. (2013)	To investigate the effects of the turbulence and radiation models on the combustion characteristics by the numerical simulations.	The predicted temperature gradients with DTRM are not agreement with experiment and simulation results published in the literature. P–I radiation model shows a better overall agreement with the experimental data and other simulation results at different axial distances	RNG k- ε, RSM (REYNOLDS STRESS MODEL)	P-1, DT (Discrete Transfer)	[22]

In this research, the key properties of radiation and its effect on flame and wall radiation have been investigated. Then, by expressing a theoretical model, the flame radiation is calculated and the measurement accuracy is compared with the theoretical model.

2. THEORETICAL ANALYSIS

To analyze the properties of radiation, it is necessary to state the desired equations. The radiation heat flux of a wall is expressed as equation (2) [23]:

$$q_{\text{net}} = \frac{\sigma(T_{\text{w}}^4 - T_{\text{m,eff}}^4)}{\frac{1}{\epsilon_{\text{m,eff}}} + \frac{1}{\epsilon_{\text{w}}} - 1} \tag{2}$$

where T_w is the wall temperature, ε_w is the amount of wall emissivity, $T_{\text{m,eff}}$ and $\epsilon_{\text{m.eff}}$ are the effective temperature and emissivity of the medium inside the chamber, respectively.

According to Kirchhoff`s law [12], in gray and diffuse systems, the wall emissivity rate is equal to the wall absorption coefficient. Therefore, the wall radiation heat flux is relative to the wall incident radiation, G_{total}, as equation (3).

$$q_{\text{net}} = \varepsilon_{\text{w}} G_{\text{total}} - \varepsilon_{\text{w}} \sigma T_{\text{w}}^4 \tag{3}$$

Considering equations (2) and (3), G_{total} could be expressed as:

$$G_{\text{total}} = \frac{\sigma(T_{\text{m,eff}}^4 - T_{\text{w}}^4)}{\frac{\epsilon_{\text{w}}}{\epsilon_{\text{m,eff}}} + 1 - \epsilon_{\text{w}}} + \sigma T_{\text{w}}^4 \tag{4}$$

where wall incident radiation, G_{total}, is the sum of the flame radiation, E_{flame}, and the sum of the emission and reflection of the wall radiation, G_{wall}, is expressed in equation (5).

$$G_{\text{total}} = G_{\text{wall}} + E_{\text{flame}} \tag{5}$$

where E_{flame} is radiation that is generated directly from the products of combustion at high temperatures and is partially absorbed and scattered by the medium, which is expressed as equation (6):

$$E_{\text{flame}} = \epsilon_{\text{m,eff}} \sigma T_{\text{m,eff}}{}^4 \tag{6}$$

and G_{wall} is a combination of wall emission and reflection. Based on equation (7), G_{wall} is expressed as the following equation.

$$G_{\text{wall}} = G_{\text{total}} - E_{\text{flame}}$$
$$\Rightarrow G_{\text{wall}} = \frac{\sigma(T_{\text{m,eff}}^4 - T_{\text{w}}^4)}{\epsilon_{\text{w}}\left(\frac{1}{\epsilon_{\text{m,eff}}} - 1\right) + 1} + \sigma T_{\text{w}}^4 - \epsilon_{\text{m,eff}} \sigma T_{\text{m ,eff}}^4 \tag{7}$$

As mentioned above, G_{wall} is a combined contribution of wall emission and reflection. It can be written as equation (8):

$$G_{\text{wall}} = G_{\text{wall,reflection}} + G_{\text{wall,emission}} \tag{8}$$

For calculating the $G_{\text{wall,reflection}}$, wall temperature should be considered zero, so:[24]

$$G_{\text{wall,reflect}} = \epsilon_{\text{m,eff}} \sigma T_{\text{m,eff}}^4 \frac{(1-\epsilon_{\text{w}})(1-\epsilon_{\text{m,eff}})}{\epsilon_{\text{w}} + (1-\epsilon_{\text{w}})\epsilon_{\text{m,eff}}} \tag{9}$$

$$G_{\text{wall,emission}} = G_{\text{wall}} - G_{\text{wall,reflect}} = \epsilon_{\text{w}} \sigma T_{\text{w}}^4 \frac{1-\epsilon_{\text{m,eff}}}{\epsilon_{\text{w}} + (1-\epsilon_{\text{w}})\epsilon_{\text{m,eff}}} \tag{10}$$

According to Equation (10), for example, as the wall temperature increases, $G_{\text{wall,emission}}$ increases. As a result, G_{wall} increases, and G_{total} increases.

3. NUMERICAL SECTION

In this paper, the steady-state combustion properties are investigated by the steady Flamelet method and the RANS1 model.

3.1 RANS equations

RANS equations are the equations of meantime for fluid flow motion. The idea behind these equations is the Reynolds discretization equation by which a moment value is subtracted from its meantime and oscillation values. The average of the governing equations of RANS is as follows [25]:

$$\text{Mass: } \frac{\partial \bar{\rho}}{\partial t} + \frac{\partial}{\partial x_i}(\rho \bar{u}_i) = 0 \tag{11}$$

$$\text{Momentum: } \frac{\partial \bar{\rho} \bar{u}_i}{\partial t} + \frac{\partial}{\partial x_i}\left(\bar{\rho} \bar{u}_i \bar{u}_j\right) + \frac{\partial \bar{p}}{\partial x_j} = \frac{\partial}{\partial x_i}\left(\bar{\tau}_{ij} - \bar{\rho} u_i'' u_j''\right) + \bar{\rho} g \tag{12}$$

Reynolds stresses ($u_i'' u_j''$) are closed by a turbulence model. With the Boussinesq relation, the Reynolds turbulence stresses can be written as follows:

$$\bar{\rho} u_i'' u_j'' = -\mu_t \left(\frac{\partial \tilde{u_i}}{\partial x_j} + \frac{\partial \tilde{u_j}}{\partial x_i} - \frac{2}{3}\delta_{ij} \frac{\partial \tilde{u_k}}{\partial x_k}\right) + \frac{2}{3}\bar{\rho} k \tag{13}$$

The term k is the turbulent kinetic energy and defined as:

$$k = \frac{1}{2}\sum_{k=1}^{3} u_k'' u_k'' \tag{14}$$

To close the additional terms generated by averaging, there is a need for additional modeling to be solved and for creating different turbulence models. In this paper, the standard turbulence model $k - \varepsilon$ is used.

The standard $k - \varepsilon$ model consists of two equations. Turbulence viscosity is expressed in this model as Equation (15).

$$\mu_t = \rho C_\mu \frac{k^2}{\varepsilon} \tag{15}$$

where C_μ is an experimental constant. k and ε are obtained with two differential equations as follow:

$$\frac{\partial}{\partial_t}(\rho k) + \frac{\partial}{\partial_{x_i}}(\rho k u_i) = \frac{\partial}{\partial_{x_i}}\left(\left(\mu + \frac{\mu_t}{\sigma_\varepsilon}\right)\frac{\partial k}{\partial x_j}\right) + G_k + G_b - \rho\varepsilon - Y_M \tag{16}$$

$$\frac{\partial}{\partial_t}(\rho k) + \frac{\partial}{\partial_{x_i}}(\rho \varepsilon u_i) = \frac{\partial}{\partial_{x_i}}\left(\left(\mu + \frac{\mu_t}{\sigma_\varepsilon}\right)\frac{\partial_\varepsilon}{\partial_{x_j}}\right) + C_{\varepsilon 1}\frac{\varepsilon}{k}(G_k + C_{\varepsilon 3}G_b) - C_{\varepsilon 2}\rho\frac{\varepsilon^2}{k} \quad (17)$$

$$G_k = -\rho u_i' u_j' \frac{\partial u_j}{\partial x_i} \quad (18)$$

where $C_{\varepsilon 1}$,$C_{\varepsilon 2}$and $C_{\varepsilon 3}$are the constant coefficient of the model. σ_ε And $\sigma_k$are turbulence numbers for ε and k, respectively. $G_k$is the term of kinetic energy production of turbulence due to medium velocity gradients. G_b is the term of turbulence in energy production. YM is the distribution of expansion oscillations in a compressive turbulence to total loss rate. In this turbulence model the constants are as follows: C_μ=0.09, $C_{\varepsilon 1}$=1.6, $C_{\varepsilon 2}$=1.92, σ_ε=1.3, σ_k=1.0.

FLUENT software is used to solve combustion equations with the applicant of the steady Flamelet method. And due to the incompressibility of the flow, the applicable solver is pressure-based and implicit.

3.2 Combustion model

In this method, the steady Flamelet method is used to model combustion. Flamelet refers to the reactive diffusive layers that are surrounded by a non-reactive flow. In the steady Flamelet method, the turbulent penetrative flame is considered as a statistical collection of Flamelets [26]. Flamelet equations are a simple form of survival equations in species and energy. The main concept of this method is based on the thinness of the reaction layer. In this method, multi-dimensional effects such as reaction scalar derivatives in the direction of the tangential flame relative to the vertical direction are ignored. It could be addressed to reference [27-29] for further investigation of Flamelet's numerical relations.

To implement the concept of a steady Flamelet for modeling a turbulent flame, a Flamelet library (including temperature distribution and mass fraction of species) is first created. Then, The Felmet equations are integrated using a chemical mechanism, and the specific dissipation rate and the mass fraction, and the steady-state temperature are obtained as a function of the mixture fraction and the scalar dissipation rate.

Once the species distribution and temperature are obtained, a database called the Flamelet Library is created. The library inputs include three parameters, mean mixture fraction, scalar dissipation rate, and mixture fraction of variance.

Survival equations which include continuity equations, momentum, intermediate fraction transfer, and variance of this quantity, are solved in the combustion chamber area using computational fluid dynamics methods. Turbulence calculations are also performed with these equations by the standard k-ε turbulence model in Fluent software. Then, with the values obtained for the average mixture fraction, the variance of this value, and the scalar dissipation rate calculated per cell, the distribution of species and temperature are read from the database. Finally, the average mass fraction of chemical species and the temperature are calculated [27-29].

3.3 Radiation model

In this study, the Discrete Ordinate (DO) radiation model is used. The DO radiation model is one of five radiation simulation models in Fluent software that uses Equation (2) to calculate the radiation heat transfer. DO model is applicable in all of the optical thickness limits and, despite the Rosseland and DTRM models, can be applied in a density-based solvent with parallel processing. The DO radiation model uses the transfer equation to absorb, emit, and scatter the medium to calculate the radiation intensity. This model solves the radiation equation for a limited number of angles. The radiation equation calculates the intensity of radiation by the method of absorption, emission, and scattering.

The equation of transfer for absorbtion, emission and scattering of the environment is [30]:

$$\frac{dI(r^{\rightarrow},s^{\rightarrow})}{ds} + (a+\sigma)I(r^{\rightarrow},s^{\rightarrow}) = an^2\frac{\sigma T^4}{\pi} + \frac{\sigma_s}{4\pi}\int_0^{4\pi} I(r^{\rightarrow},s'^{\rightarrow})\phi(s^{\rightarrow},s'^{\rightarrow})d\omega' \quad (19)$$

In this equation, $r^{\rightarrow}$ is the position vector, $s^{\rightarrow}$ is the direction vector, $s'^{\rightarrow}$ is the vector of scattering direction, s is the length direction, a is the absorption coefficient, n is the fraction coefficient, σ_s is the scattering coefficient, ω' is the spatial angle and φ is phase function. The phase function is an angular discretization of scattered radiation intensity by the particles at a specific wavelength. The phase function can be expressed as the intensity of scattered radiation in a certain direction relative to the total intensity of scattered radiation in all directions.

3.4. Physical domain

In this paper, a can-type combustion chamber is studied. Its length is 210 mm, and its maximum width is 75 mm. The circular shape at the end of this combustion chamber has changed to a square with a length of 100 mm and a width of 25 mm. A swirler with 20 blades and approximately one swirl number is installed in the above combustor. This is a high swirl number. This swirler has an inner diameter of 10.81 mm, an outer diameter of 16.15 mm, and a length of 15 mm. The diameter of the casing is 162 mm, and the combustion chamber is located inside it. The thickness of the case(body) is 5 mm. The combustion chamber diameter is 74 mm, and its thickness is 2 mm. The air inlet volume of the case inside is 170 m^3/hr, and the amount of fuel injected into the combustor is 3.9 lit/hr. Two rows of holes are installed on this combustion chamber. The first row has 6 holes and the second row has 12 holes. The diameter of all holes is 10 mm. Approximately 37% of the air inlet through the combustion chamber is from the swirler, 20% from the first row, and 43% from the second row [31]. Figure 1 shows an overview of the simulated combustion chamber and the specifications of the simulated combustion chamber.

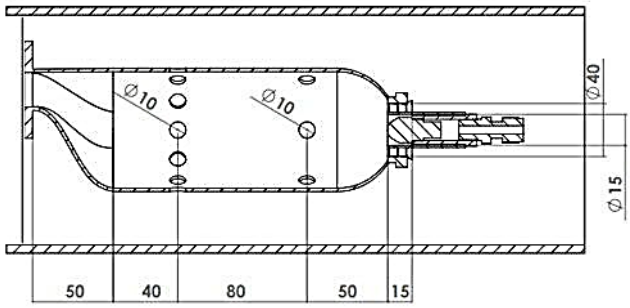

Figure1 overview of the simulated combustion chamber

3.5. Computational domain

Figure 2 shows the computational domain. To determine the boundary conditions, the fuel inlet and fuel mass fraction are assumed to be unique, and the fuel inlet temperature is 300 K in each condition. The pressure gradient at the inlet is assumed zero. The boundary conditions of this study are shown in Table 1.

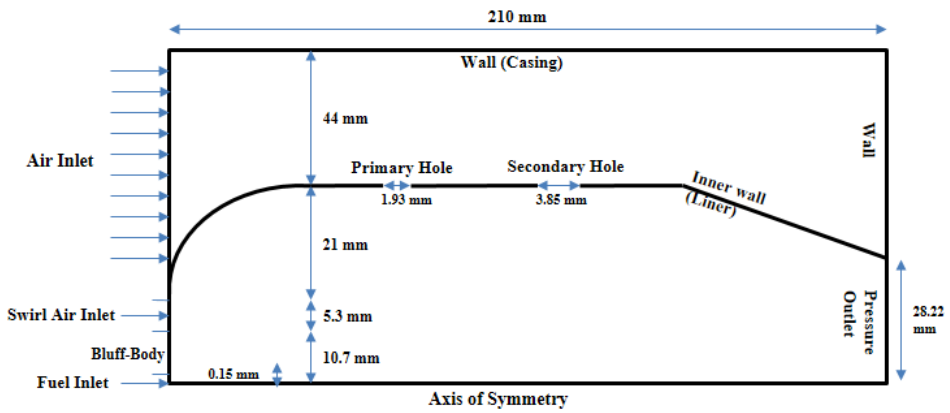

Figure2 Simulated combustion chamber specifications

Table1 boundary conditions

Fuel Inlet	Air Inlet	Outlet	Bluff body	Casing
Mass Flow Inlet	Mass Flow Inlet	Pressure Outlet	Wall	Wall

The fuel used in this simulation is liquid kerosene with the chemical formula $C_{10}H_{20}$. Arrhenius coefficients are used to calculate the amount of production and consumption species [32,33]. The Discrete Phase Model (DPM) method is used to simulate liquid fuel spray modeling in the chamber. In this method, the Pressure-Swirl-Atomizer model is selected as the fuel spray. By determining the spray angle and upstream pressure, the fuel enters the chamber, and after calculating the forces on the fuel droplets, they begin to evaporate. Finally, the combustion flow of the output from the outlet and the numerical field is completed.

In the simulation, a pressure-based solver is used in the implicit method with asymmetric axis swirl space and fixed time. The SIMPLE method is also used to connect the pressure to the velocity field.

Table 2 shows the inlet characteristics of the combustion chamber. $\dot{m}_s$ is the mass flow of swirl air that enters the combustion chamber, $\dot{m}_a$ is the mass flow of air that passes through the combustion chamber and enters the chamber through the holes around the shell. $\dot{m}_f$ is the fuel mass flow that enters through the injector.

Table2 Physical characteristics of the combustion chamber

Fuel	$\dot{m}_s$**(kg/s)**	$\dot{m}_a$**(kg/s)**	$\dot{m}_f$**(kg/s)**	**Spray half angle(degree)**	**Injector inner diameter(mm)**
$C_{10}H_{20}$	0.124	0.0243	0.0009	40	0.3

4. RESULT AND DISCUSSION

In this section, simulation results are presented. First, the independence of the grid is examined. Then, the effect of wall temperature on flame radiation is studied. Then, the effect of the gas scattering coefficient on flame radiation and radiation heat flux is investigated. Finally, a radiation model is presented and compared with numerical simulation results. Table 3 summarizes the simulation.

Table 3 simulation summary

Case No.	**aim**	**Gas scatter coef.**	**Wall Temp.**
Case 1	effect of wall temperature on the flame radiation	1	298 489 800 1000
Case 2	Effect of the gas scattering coefficient on the flame radiation	0 1 10 100	298
Case 3	Radiation heat flux	0 1 10 100	298

4.1 Grid dependency and validation

Three structured computational networks have been used to examine the grid's independence. Table 4 shows the number of grid cells. Figures 3, 4, and 5 show the axial velocity, temperature, and mass fraction distribution of CO_2 for the three computational grids. As shown in these graphs, the results are independent of computational grids. The effect of grid change with more than 141,810 nodes is almost negligible. Therefore, a computational grid with 141,810 nodes has been selected for the study.

Table 4 The Grids examined for optimal Grid selection

	grid1	grid2	grid3
Number of nodes	67016	143688	210337
Number of cells	65,824	141,810	207,999

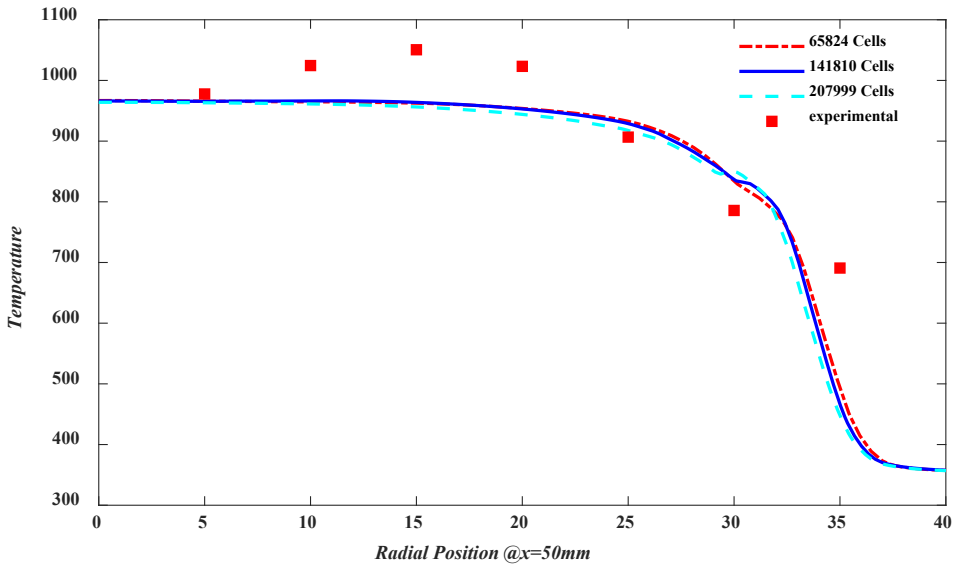

Figure3 Comparison of temperature variations for three computational grids at x = 50mm with experimental model [34]

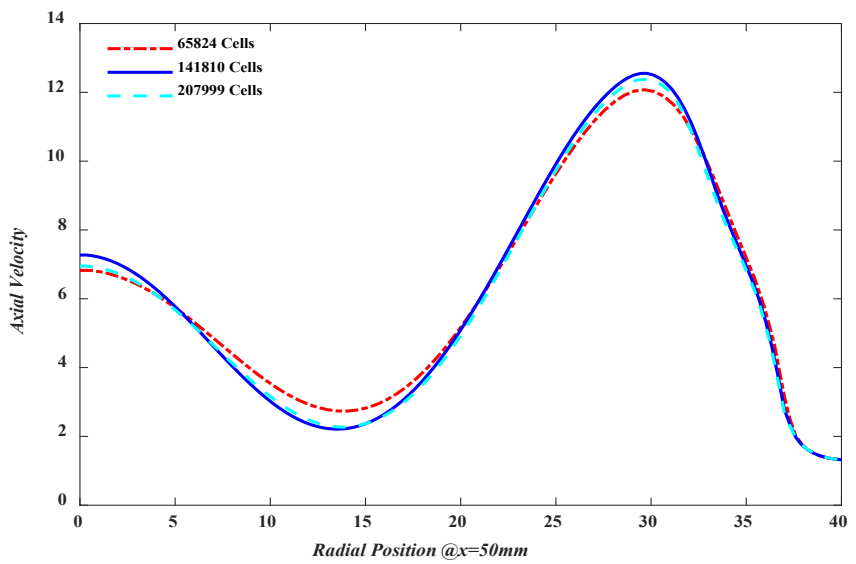

Figure 4 Comparison of axial velocity variations for three computational grids at x = 50mm

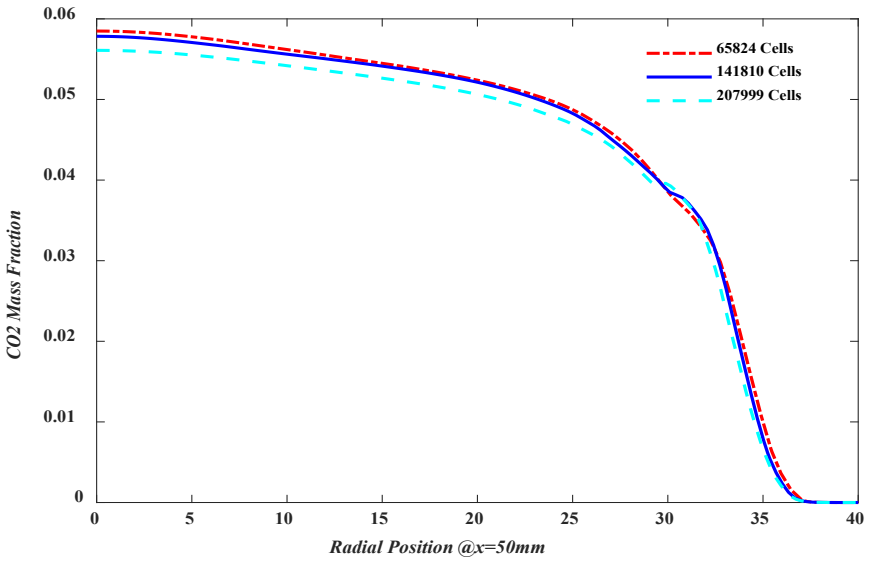

Figure 5 Comparison of CO2 mass fraction variations for three computational grids at x = 50mm

4.2. Effect of wall temperature on flame radiation

In this section, the effect of radiation heat transfer on the combustion chamber is studied. The material of the combustion chamber body is 310 steel alloy, and its emissivity is 0.9. First, the effect of wall temperature is studied. For evaluation, it applied in four cases of wall temperatures which are 298K, 489K, 800K, and 1000K.

Due to the direct effect of the outer wall temperature (casing) on the radiation temperature inside the combustion chamber, with increasing temperature on the casing, which corresponds to Equation 5, the incident radiation on the inner wall (liner) increases. This phenomenon is shown in Figure 6. In this way, it shows two fraction points at x = 50 mm and x = 100 mm, which represent the primary and secondary holes in the liner wall, respectively. And due to the entry of colder air into those holes, the wall temperature and radiation temperature are lower in these places. Therefore, incident radiation in that area is reduced.

As shown in Figure 6, an increase in temperature increases the incident radiation on the combustion chamber liner wall. The same is true for the casing. As shown in Figure 7, incident radiation on the casing increases with increasing casing temperature.

Figure 8 shows the effect of the casing temperature on the radiation heat flux of the liner wall. As can be seen, the increase in the casing temperature has increased the heat flux of the inner wall radiation. Minimizing this value means increasing the radiation flux that passes out of the liner wall to the casing. This study was also performed on the casing, as shown in Figure 9. In this figure, the positive values are due to the absorption of radiation heat flux by the casing.

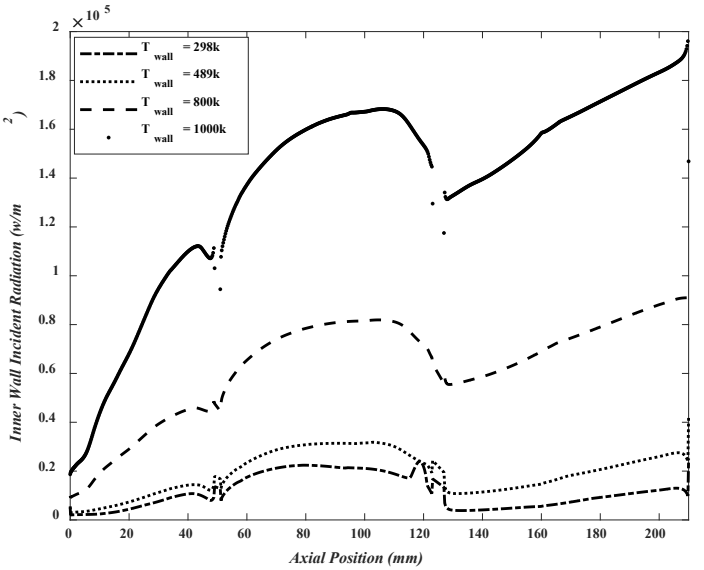

Figure 6 Effect of External wall (casing) temperature changes on the internal wall (liner) radiation relative to the longitudinal axis

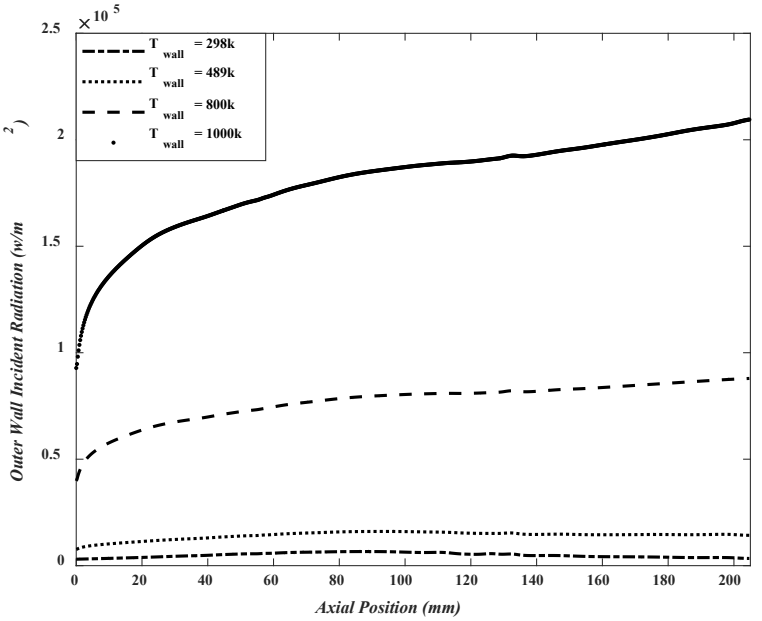

Figure 7 Effect of casing temperature changes on the casing radiation relative to the longitudinal axis

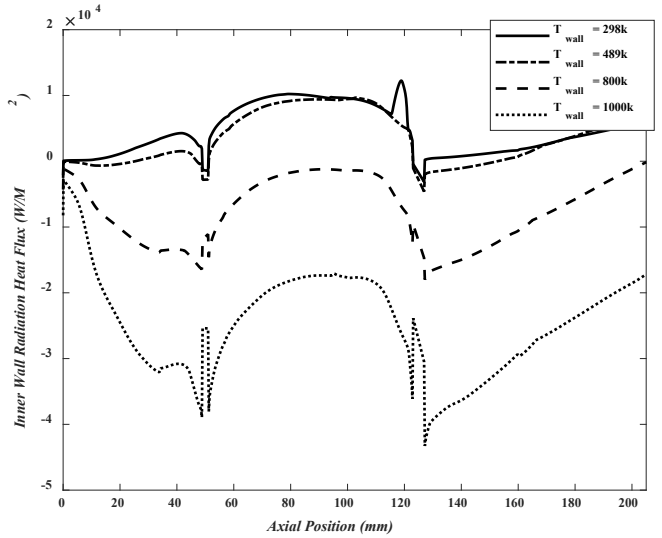

Figure 8 Effect of the casing temperature changes on the liner radiation heat flux

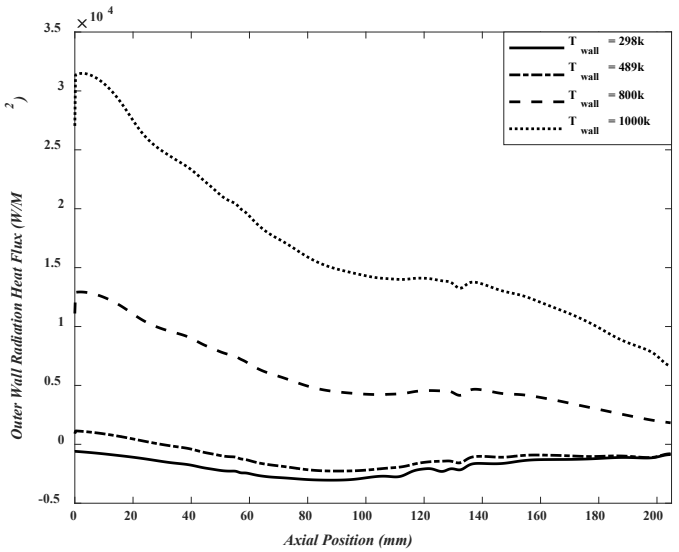

Figure 9 Effect of casing temperature changes on casing radiation heat flux

Thermal radiation is electromagnetic radiation that is generated by the thermal motion of charged particles in matter. All materials emit thermal radiation at temperatures above absolute zero. Thermal radiation temperature is commonly known as radiation temperature.

The radiation temperature and the static temperature of the combustion chamber are shown in Figures 10 a and b, respectively. Comparing these two temperatures in these figures shows that radiation heat transfer in the combustion chamber and between the two inner and outer walls is very effective in the overall heat transfer. In static temperature contours, the effect of the cold air intake on the convection heat transfer between the internal and external walls is obvious, which reduces the temperature in the external wall. But in radiation temperature contours, the heat transfer of radiation is independent of air entrance, therefore, the radiation temperature has more effect on the casing of the combustion chamber.

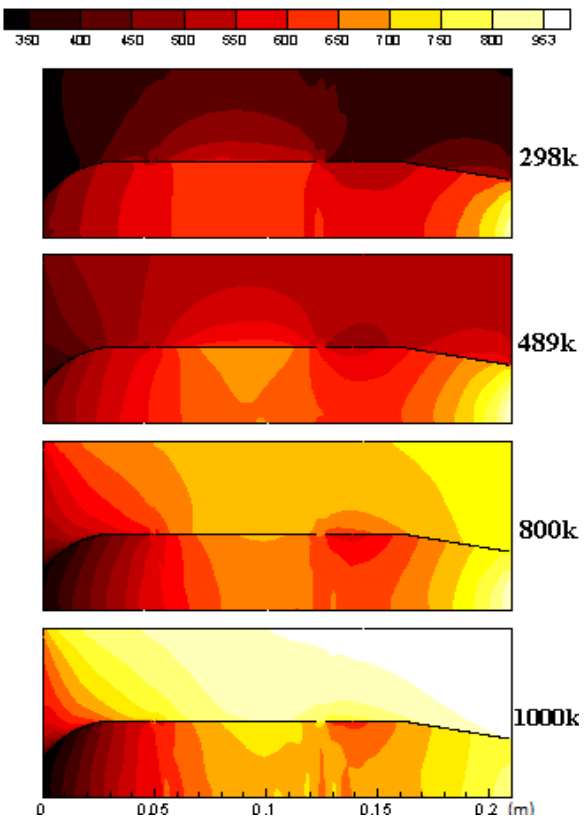

(a)

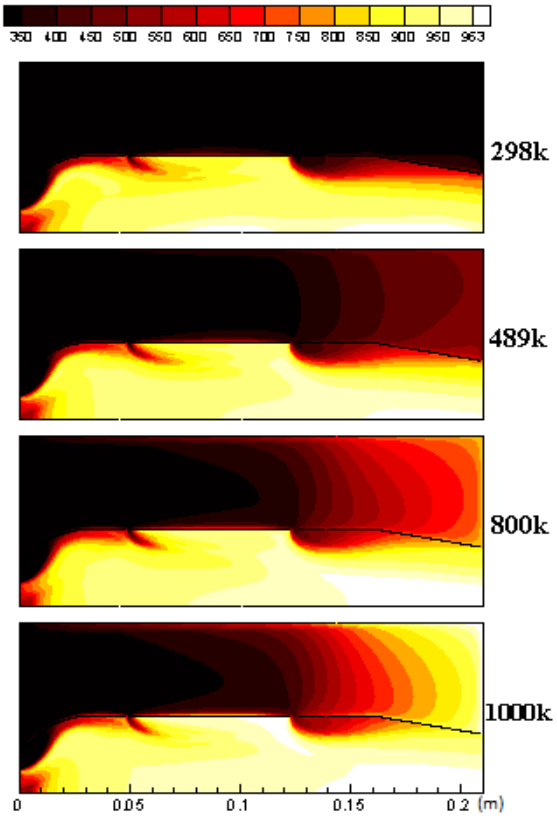

(b)

Figure 10 (a) Radiation temperature contours and (b) static temperature contours at various casing temperatures 289, 489, 800 and 1000K

4.3. Effect of the gas scattering coefficient on flame radiation

Considering the equation of transfer for absorption, emission, and scattering of the environment described earlier, it can be written as [23]:

$$\frac{dI'_\lambda}{ds} = -K_\lambda(\mathrm{s})\, \mathrm{I}'_\lambda(\mathrm{s}) + \mathrm{a}_\lambda(\mathrm{s})\, \mathrm{I}'_{\lambda \mathrm{b}}(\mathrm{s}) + \frac{\sigma_{s\lambda}}{4\pi} \int_{\omega_{i=0}}^{4\pi} I'_\lambda(s, \omega_i) \varphi(\lambda, \omega, \omega_i) d\omega_i \qquad (20)$$

where $K_\lambda(\mathrm{s})$ is the extinction coefficient equal to the total gas absorption coefficient and the scattering coefficient:

$$-K_\lambda(\mathrm{s})\, \mathrm{I}'_\lambda(\mathrm{s}) = -\mathrm{a}_\lambda(\mathrm{s}) \mathrm{I}'_\lambda(\mathrm{s}) - \sigma_{s\lambda}(s) \mathrm{I}'_\lambda(\mathrm{s}) \qquad (21)$$

Thus, Equation (20) is divided into four parts:

1) Reduction effect due to gas absorption: $dI'_{\lambda,a} = -\mathrm{a}_\lambda(\mathrm{s}) \mathrm{I}'_\lambda(\mathrm{s})\, \mathrm{ds}$
2) Reduction effect due to gas scattering: $dI'_{\lambda,s} = -\sigma_{s\lambda}(\mathrm{s}) \mathrm{I}'_\lambda(\mathrm{s}) \mathrm{ds}$
3) Incremental effect due to radiation emitted from the gas itself: $dI'_{\lambda,s} = \mathrm{a}_\lambda(\mathrm{s})\, \mathrm{I}'_{\lambda \mathrm{b}}(\mathrm{s})$
4) Incremental effect due to environmental scattering: $dI'_{\lambda,s} = \frac{\sigma_{s\lambda}}{4\pi} \int_{\omega_{i=0}}^{4\pi} I'_\lambda(s, \omega_i) \varphi(\lambda, \omega, \omega_i) d\omega_i$

Flame temperature contours in different scattering coefficients (σ = 0,1,10,100) are presented in Figure 12. As observed, the temperature changes in the chamber remain almost constant as the scattering coefficient increases. Because according to the equation of transfer in the DO radiation model, incident radiation decreases with increasing gas scattering (the second part of the equation), which is a decreasing part. But due to part 4 of equation (20), increasing the scattering increases part 4 of the equation. As a result, the effect of reduced incident radiation due to the increase in gas scattering is neutralized, and the flame temperature changes remain constant. Figure 12 shows the flame temperature contours at different scattering coefficients of 0, 1, 10, and 100. According to the figure, the effect of scattering coefficient changes on flame temperature changes is negligible.

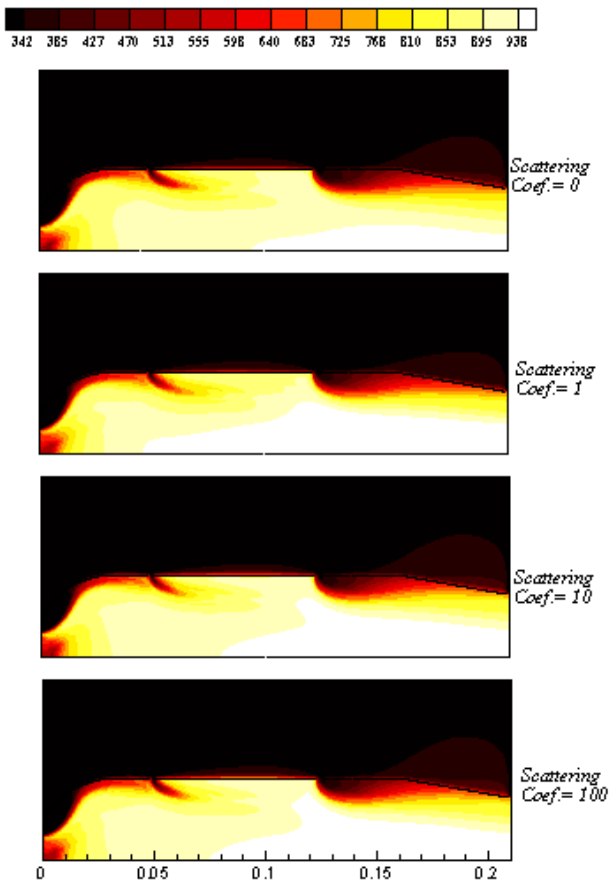

Figure 12 Flame Temperature (K) contours at different Scattering Coefficients (σ = 0,1,10,100)

As mentioned, the extinction coefficient increases with increasing scattering coefficient. And since the optical thickness according to the following equation is directly related to the extinction coefficient:

$$k_\lambda(s) = \int_0^s K_\lambda(s)ds \tag{22}$$

where $k_\lambda(s)$ is optical thickness and $K_\lambda(s)$ is the extinction coefficient. As a result, the optical thickness increases, and according to the equation of transfer, incident radiation increases with increasing optical thickness.

Figure 13 shows the incident radiation in different scattering coefficients. As shown in the figure, the effect of radiation in the combustion chamber increases with an increasing scattering coefficient. And according to Figure 14, the incident radiation of the wall has increased with increasing gas scattering coefficient.

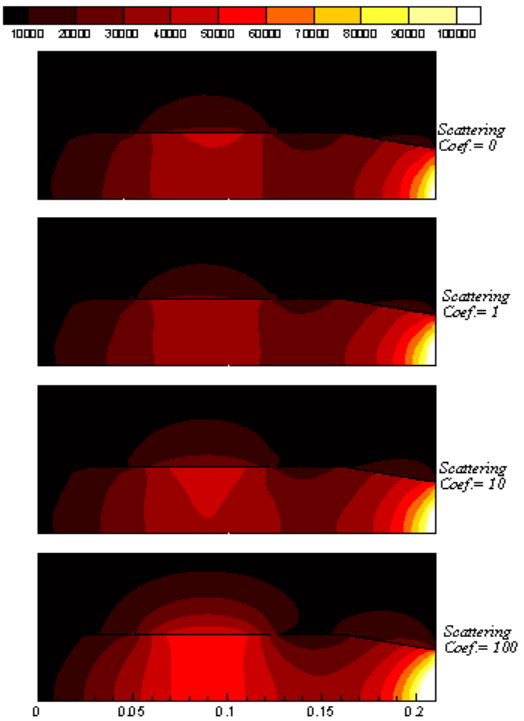

Figure 13 Incident radiation contours at various scattering coefficients (σ = 0,1,10,100)

In Figure 15, the radiation heat flux of the inner wall decreases with an increasing scattering coefficient. The negative sections of the plot are due to the heat radiation flux since the effective temperature ($T_{m,eff}$ in equation (3) is higher than the wall temperature in that part (the temperature of the liner wall varies). As the scattering coefficient increases, the radiation temperature increases and thus the effective temperature. As the effective temperature increases, the difference between the effective temperature and the wall temperature decreases in different parts of the wall. Then, the heat flux of the wall radiation decreases, and if this difference increases, due to the more positive or negative difference, the flux of radiation heat transfer becomes more positive or negative.

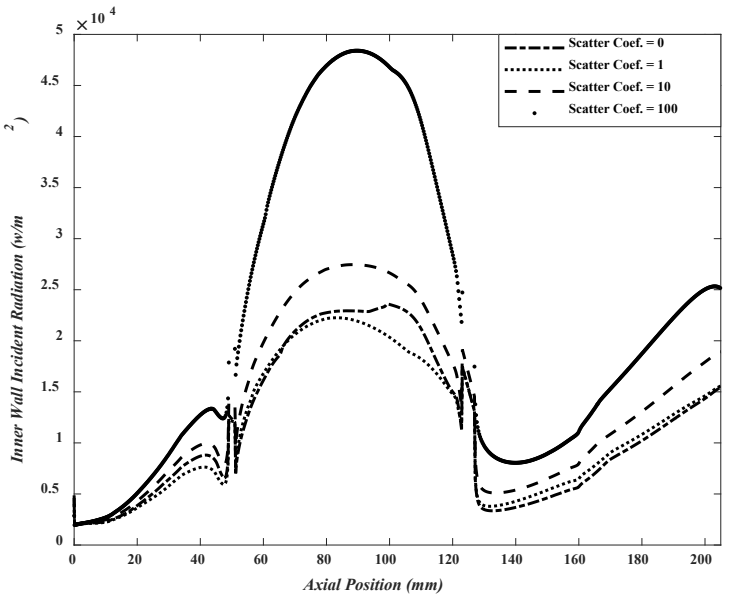

Figure 14 Incident radiation changes to the liner (W/m^2) in different scattering coefficients (σ = 0,1,10,100)

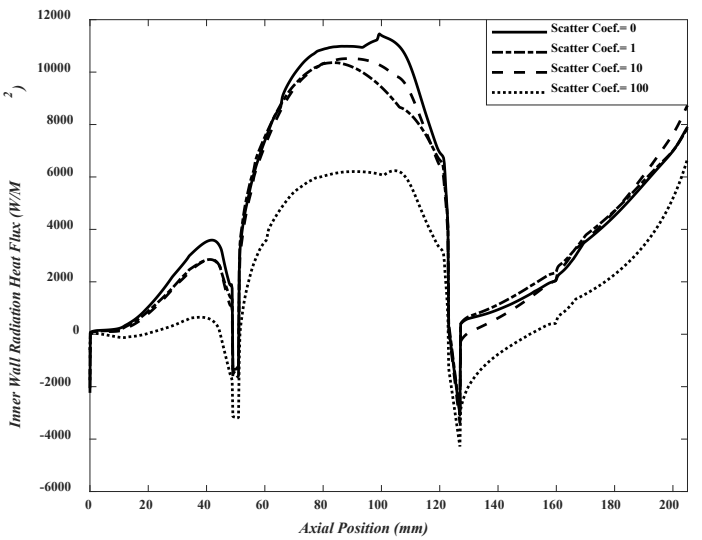

Figure 15 radiation heat flux changes to the liner in different scattering coefficients (σ = 0, 1, 10,100)

4.4. radiation model and comparison with numerical simulation results

In this section, the effects of wall radiation on flame radiation in four cases are compared in two numerical methods (using the radiation relations expressed in the previous sections) and simulation in Fluent software. Then, the results are presented in a plot for all modes. With the results presented in the previous sections, the change in the extinction coefficient and the shape of the flame at different wall temperatures were almost negligible. Therefore, it can be concluded that the flame radiation is equal to the value for the four items listed in Table 5. This result helps to measure the effect of wall radiation on the flame with the same property.

In this case, four different types of walls, each with its radiation and temperature, have been examined. Table 5 shows each of its characteristics of wall temperature, wall emissivity, and liner wall incident radiation of the simulation for four different modes at a distance of x = 100 mm on the wall. Using Equation G_{total} and two cases in Table 5 (ϵ_w and T_w), the values of $\epsilon_{m,eff}$ and $T_{m,eff}$ can be obtained by solving two equations and two unknowns. And the effective temperature and emissivity of the medium can be solved for the following: $\epsilon_{m,eff} = 0.955$, $T_{m,eff} = 964\,K$. Flame radiation can be obtained based on these two parameters: $E_{flame} = \epsilon_{m,eff}\sigma {T_{m,eff}}^4 = 46762 \frac{w}{m^2}$. Table 5 also predicts the amount of deviation due to the difference between wall radiation and flame radiation. By specifying the values $\epsilon_{m,eff}$ and $T_{m,eff}$, the value of G_{total} can be calculated for all wall conditions. In Figure 16, using $\epsilon_{m,eff} = 0.955$ and $T_{m,eff} = 964K$ the predicted values of G_{total} are plotted using the theoretical model (equation 5) and compared with simulation values at several points. According to G_{total} equation (5), the value of E_{flame}(equation 7) is equal to the amount of incident radiation emitted from the liner wall when the wall emissivity is equal to 1, and the wall temperature is zero. the difference between flame radiation and wall radiation in all wall temperature ranges is less than 10%.

Table 5 effect of wall emissivity variation on simulation result by changing the type of the wall

Wall type	**Stainless steel 310 (25% Cr, 20% Ni)**	**Steel Aluminized**	**Stainless steel 304 (8% Cr, 18% Ni)**	**Steel Alloyed (18%Cr, 8% Ni)**
emissivity, $\boldsymbol{\epsilon_w}$	0.9	0.79	0.44	0.35
casing temperature, $\boldsymbol{T_w}$ (k)	489	323	489	773
Predicted of liner wall incident radiation by the theoretical method, Gtotal (w/m2)	47105	47230	48037	48500
$\%\frac{\textbf{wall radiation}-\textbf{flame radiation}}{\textbf{falme radiation}}$	0.73	1	2.73	3.58

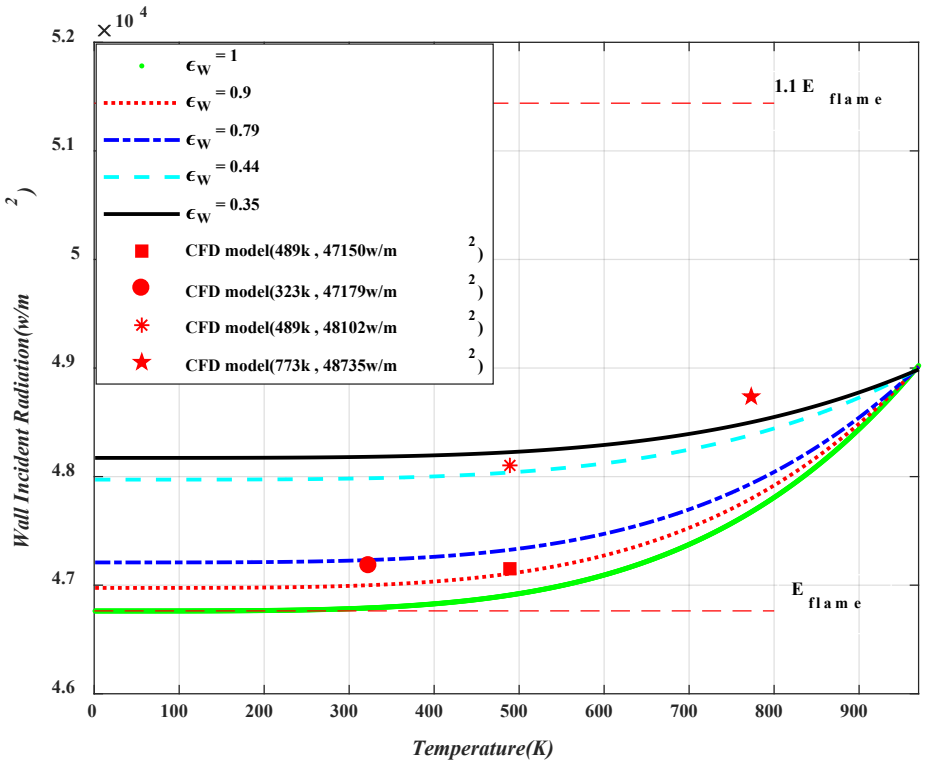

Figure 16 the variations in predicted liner incident radiation by theory model (lines) and simulated liner incident radiation (symbols) at x=100mm

5. CONCLUSION

A can type gas turbine combustion chamber simulated using RANS and steady Flamelet combustion model. Comparison of gas temperature results with experimental results showed the accuracy of simulation settings. Due to the low optical thickness of the model, the DO radiation model was implemented. Variation in radiation parameters was investigated, and the effect of the wall on flame radiation was determined. The results of this paper can be summarized as follows.

As the casing temperature increases, the liner wall incident radiation increases, and with increasing the wall emissivity, the surface incident radiation decreases. As a result, to minimize the effect of the wall on flame radiation, it must be at a low temperature and high emissivity, although it can not occur simultaneously.

Increasing the scattering coefficient increases the radiation temperature and surface incident radiation. Furthermore, inner wall radiation heat flux also increases.

In this study, using the numerical method for a point on the wall of the combustion chamber, $T_{\mathrm{m,eff}}$ and $\epsilon_{\mathrm{m,eff}}$ were , and based on them, the flame radiation was calculated. Also, wall incident radiation was predicted and shown for specific wall emissivity. For evaluation, using wall incident radiation simulated with Fluent at a specific point on the wall and different emissivities, it was evaluated in a plot that matched the predicted wall incident radiation, G_{total}.

Different steel alloys with different emissivities for the combustion chamber are evaluated. As results showed, in this type of combustion chamber, the deviation between the flame radiation and the wall in all ranges of wall temperature was less than 10%.

6. REFERENCES

[1] C. Tien, S. Lee, Flame radiation, Progress in Energy and Combustion Science,8,pp.41–59, 1982.

[2] R. Viskanta, M. Mengüç, Radiation heat transfer in combustion systems, Progress in Energy and Combustion Science, 1987.

[3] K. Zhou, N. Liu, L. Zhang, K. Satoh, Thermal radiation from fire whirls: revised solid flame model, Fire technology;50, pp.1573–87, 2014.

[4] ES. Oran, JP. Boris, Detailed modeling of combustion systems, Progress in Energy and Combustion Science;7,pp.1–72, 1981.

[5] P. Nakod, G. Krishnamoorthy, M. Sami, S. Orsino, A comparative evaluation of gray and non-gray radiation modeling strategies in oxy-coal combustion simulations, Applied Thermal Energy, 54, pp.422–32, 2013.

[6] AA. Bhuiyan, J. Naser, Numerical modeling of oxy-fuel combustion, the effect of radiative and convective heat transfer and burnout, Fuel, 139, pp.268–84, 2015.

[7] F. Xia, Z. Yang, A. Adeosun, BM. Kumfer, RL. Axelbaum, Staged, pressurized oxy-combustion: computational fluid dynamic simulations z boilers, The 8th international symposium on coal combustion, Beijing, China, 2015.

[8] J. Zhang, T. Ito, S. Ito, D. Riechelmann, T. Fujimori, Numerical investigation of oxy-coal combustion in a large-scale furnace: non-gray effect of gas and role of particle radiation, Fuel, 139, pp.87–93, 2015.

[9] D. Woycenko, W. Van de Kamp, P. Roberts, Combustion of pulverized coal in a mixture of oxygen and recycled flue gas, Summary of the APG research program, IF8RF Doc, in, F98/Y/4. Ijmuiden, The Netherlands: International Flame Research Foundation (IFRF), 1995.

[10] B. Kashir, S. Tabejamaat, and N. Jalalatian, A numerical study on combustion characteristics of blended methane-hydrogen bluff-body stabilized swirl diffusion flames, International Journal of Hydrogen Energy 40,18, pp. 6243-6258, 2015.

[11] F. Fasihi, S. Noori, M. Eidi Attar Zadeh, Investigation of radiative heat transfer effect on the SM1 flame structure with steady flamelet method, Modares Mechanical Engineering, Vol.18, No. 04, pp. 397-208, 2018 (in Persian)

[12] Mohammad Raghib Shakeel, Yinka S. Sanusi, Esmail M. A. Mokheimer, Numerical Modeling of Oxy-Fuel Combustion in a Model Gas Turbine Combustor: Effect of Combustion Chemistry and Radiation Model, 9th International Conference on Applied Energy,Vol.142,pp. 1647–1652, 2017.

[13] Ernesto Benini, Sergio Pandolfo, Serena Zoppellari, Reduction of NO emissions in a turbojet combustor by direct water/steam injection: Numerical and experimental assessment, Applied Thermal Engineering, 29, pp.3506–3510, 2009.

[14] Felipe Roman Centeno, Rogério Brittes, Francis H.R. França, Cristiano Vitorino da Silva, Application of the WSGG model for the calculation of gas–soot radiation in a turbulent non-premixed methane–air flame inside a cylindrical combustion chamber, International Journal of Heat and Mass Transfer, 93, pp.742–753, 2016.
[15] A. Datta, S.K. Som, Combustion and emission characteristics in a gas turbine combustor at different pressure and swirl conditions, Applied Thermal Engineering, 19, pp. 949-967, 1999.
[16] Nimeti Doner, Nevin Selçuk, "An application of Spectral line-based weighted sum of grey gases (SLW) model with geometric optics approximation for radiative heat transfer in 3-D participating media, Applied Thermal Engineering, 50, pp. 89-93, 2013.
[17] Gautham Krishnamoorthy, A computationally efficient P1 radiation model for modern combustion systems utilizing pre-conditioned conjugate gradient methods, Applied Thermal Engineering, 119 pp.197–206, 2017.
[18] Parag Rajpara, Ankit Dekhatawala, Rupesh Shah, Jyotirmay Banerjee, Thermal and emission characteristics of reverse air flow CAN combustor, International Journal of Thermal Sciences, 2018; https://doi.org/10.1016/j.ijthermalsci.2017.12.008.
[19] N.Y. Sharma, S.K. Som, Influence of fuel volatility and spray parameters on combustion characteristics and NO emission in a gas turbine combustor, Applied Thermal Engineering, 24, pp. 885–903, 2004.
[20] Wei Yang, Aiwu Fan, Jianlong Wan, Wei Liu, Effect of external surface emissivity on flame-splitting limit in a micro cavity-combustor, Applied Thermal Engineering, 83, pp. 8-15, 2015.
[21] Zhi Yi, Zhenggang Su, Qiangda Yang, Guojun Li, Weijun Zhang, Study of the non-gray-TRI effect on the turbulent methane combustion under O2/CO2 atmosphere, Applied Thermal Engineering, 130, pp.449–457, 2018.
[22] Ilker Yilmaz, Murat Tas_tan, Mustafa Ilbas, Cevahir Tarhan, Effect of turbulence and radiation models on combustion characteristics in propane–hydrogen diffusion flames, Energy Conversion and Management, 72, pp.179–186, 2013.
[23] FP. Incropera, Fundamentals of heat and mass transfer, John Wiley & Sons, 2011.
[24] Zhiwei Yang, Adewale Adeosun, Benjamin M. Kumfer, Richard L. Axelbaum, An approach to estimating flame radiation in combustion chambers containing suspended-particles, Fuel,2017;
[25] Poinsot T, Veynante D. Theoretical and numerical combustion. 2nd ed. United States of America: Edwards; 2000.
[26] N. Peters, Laminar Diffusion Flamelet Models in Non-premixed Turbulent Combustion, Progress in Energy and Combustion Science, 3, pp. 319-339, 1984.
[27] Pitsch H, Barths H, Peters N. Three-dimensional modeling of NO and soot formation in DI diesel engines using detailed chemistry based on the interactive flamelet approach. SAE Tech Pap 962057; 1996.
[28] Bray K, Peters N. Laminar flamelets in turbulent flames. In: Libby P, Williams F, editors. Turbulent reacting flows. New York: Academic Press. pp. 78-84; 1994.
[29] Marracino B, Lentini D. Radiation modeling in non-luminous non-premixed turbulent flames. Combust Sci Technol.128:23-48;1997.
[30] Robert Siegle, John.R Howel, Thermal Radiation Heat Transfer, Lewis Research Center, Government printing Office,Washington, NASA SP- 164, Vol.3,1971.

[31] Heitor, M. V., & Whitelaw, J. H. (1986). “Velocity, temperature, and species characteristics of the flow in a gas turbine combustor”, Combustion and Flame, 64(1), 1-32.

[32] Chi-Ming Lee, Krishna Kundu, “Simplified Jet-A Kinetic Mechanism For Combustor Application”, NASA Technical Memorandum 105940, AIAA-93-0021.

[33] Bonnie J.Mcbride, “Coefficient For Calculating Thermodynamic And Transport Properties Of Individual Species”, NASA Technical Memorandum 4513.

[34] Seyed MohammadReza SadatAkhavi, Sadegh Tabejamaat, Masoud EiddiAttarZade, Benyamin Kankashvar, Experimental and numerical study of combustion characteristics in a liquid fuel CAN micro-combustor, Aerospace Science and Technology,2020.